

1 **Influence of PPh3 moiety in the anticancer activity of neworganometallic ruthenium complexes**

2
3
4
5
6 Rubén Sáez ^a, Julia Lorenzo ^b, Ma Jose Prieto ^c, Mercè Font-Bardia ^d, Teresa Calvet ^d, Nuria Omeñaca ^e,
7 Marta Vilaseca ^e, Virtudes Moreno ^{a,*}
8
9
10
11
12
13
14
15
16
17
18
19
20

21 a Department de Química Inorgànica, Facultat de Química, Universitat de Barcelona, Martí y Franquès
22 1-11, 08028 Barcelona, Spain

23 b Institut de Biotecnologia i Biomedicina, Universitat Autònoma de Barcelona, 08193 Barcelona, Spain

24 c Departament de Microbiologia, Facultat de Biologia, Universitat de Barcelona, Diagonal 645, 08028
25 Barcelona, Spain

26 d Departament de Cristal·lografia, Mineralogia i Dipòsits Minerals, Universitat de Barcelona, Martí i
27 Franquès s/n., 08028 Barcelona, Spain

28 e IRB Barcelona-Institute for Research in Biomedicine, Parc Científic de Barcelona, Baldiri Reixac, 10-
29 12, 08028 Barcelona, Spain
30
31
32
33
34

35 * **Corresponding author.**

36
37 E-mail address: virtudes.moreno@qi.ub.es (V. Moreno).
38
39
40

41 **Keywords:** Arene ruthenium(II) complexes Ruthenium antitumor compounds pBR322 DNA Calf
42 thymus DNA DNA interaction Protein interaction
43
44
45
46

47 **ABSTRACT**

48

49 The effect of the PPh₃ group in the antitumor activity of some new organometallic ruthenium(II)
50 complexes has been investigated. Several complexes of the type [Ru(II)(Cl)(PPh₃)(Lig-N)],
51 [Ru(II)(Cl)₂(Lig-N)] (where Lig-N= pyridine derivate) and [Ru(II)(Cl)(PPh₃)₂], have been synthesized
52 and characterized. A noticeable increment of the antitumor activity and cytotoxicity of the complexes
53 due to the presence of PPh₃ moiety has also been demonstrated, affording IC₅₀ values of 5.2 μM in HL-
54 60 tumor cell lines. Atomic force microscopy, circular dichroism and electrophoresis experiments have
55 proved that these complexes can bind DNA resulting in a distortion of both secondary and tertiary
56 structures. Ethidium bromide displacement fluorescence spectroscopy studies and viscosity
57 measurements support that the presence of PPh₃ group induces intercalation interactions with DNA.
58 Indeed, crystallographic analysis, suggest that intra-molecular π-π interactions could be involved in the
59 intercalation within DNA base pairs. Furthermore, high performance liquid chromatography mass
60 spectrometry (HPLC-MS) studies have confirmed a strong interaction between ruthenium complexes
61 and proteins (ubiquitin and potato carboxypeptidase inhibitor — PCI) including slower kinetics due to
62 the presence of PPh₃ moiety, which could have an important role in detoxification mechanism and others.
63 Finally, ion mobility mass spectrometry (IMMS) experiments have proved that there is no significant
64 change in the gas phase structural conformation of the proteins owing to their bonding to ruthenium
65 complexes.

66

67

68

69

70 1. INTRODUCTION

71

72 In the last few years, ruthenium complexes have attracted much attention as building blocks for new
73 transition-metal-based antitumor agents, since they present some advantages over platinum complexes
74 currently used in cancer chemotherapy [1,2]. Ruthenium compounds show less toxicity, a novel
75 mechanism of action, the prospect of noncross-resistance [3,4] and a different spectrum of activity [5,6].
76 More concretely, organometallic ruthenium(II) complexes with arene ligands represent an important
77 group of ruthenium compounds with anticancer activity that is being intensively studied in the last
78 decades [7]. The typical structure of organometallic ruthenium complexes bearing η^6 -arene ligands is
79 shown in Fig. 1, which consist in a half-sandwich “piano-stool” $[(\eta^6\text{-arene})\text{Ru}(\text{X})(\text{Y})(\text{Z})]$ complex,
80 where X is usually a monodentate leaving group and Y, Z can be monodentate or chelating ligands,
81 depending on the purpose of the design [8,9].

82 These half sandwich “piano-stool” type constructs offer much scope for design, with the potential for
83 modifications to the arene and its substituents (R), the monodentate leaving group (X), the ligands Y and
84 Z, and overall charge of the complex ($n+$). These features provide handles for the control of both the
85 thermodynamics and kinetics of these systems as well as their overall structural architecture, allowing a
86 more rational drug design approach compared to platinum-based drugs [10]. They also provide an ability
87 to fine-tune the chemical reactivity of the complexes, potentially allowing the control of
88 pharmacological properties including cell uptake, distribution, and interactions with biomolecules, toxic
89 side effects, and detoxification mechanisms [11].

90 With regard to their mechanism of action, the role of the arene moiety, as well as the influence of the
91 other ligands on the aqueous chemistry of several complexes have been widely investigated [12–18],
92 resulting in a complex structure–activity relationship [7]. As observed for other ruthenium complexes,
93 their cytotoxicity is usually correlated with DNA binding [19–21], although recent works point to other
94 biomolecules as possible biological targets. As an example, RAPTA complexes do not show selective
95 binding to DNA *in vitro*, and proteins and RNA appear to be the main intracellular targets [22]. In the
96 same way, in the case of the NAMI-A antimetastatic agent, it is apparent that DNA is not the target, and
97 more likely, activity is a consequence of drug–protein interaction. This is especially interesting since the
98 antimetastatic behavior is not unique to NAMI-A, but applicable to other classes of ruthenium
99 complexes [23,24]. Related to these results, here we explore the interaction of η^6 -arene ruthenium(II)
100 complexes with some specific proteins.

101 Lastly, previous works suggest that the addition of the hydrophobic PPh₃ ligand in RAPTA complexes
102 results in more cytotoxic and less selective drugs, presumably because of increased drug uptake [22].

103 With the aim of developing more potent anticancer drugs, we have synthesized and characterized six
104 new organometallic arene–ruthenium(II) complexes, some of them including PPh₃ group in its structure.
105 In this work we study the influence of tri-phenyl-phosphine moiety in the antitumor activity of several
106 η^6 -arene ruthenium(II) complexes, and try to elucidate the possible reason behind this phenomenon.

107

108 2. EXPERIMENTAL

109

110 2.1. Materials

111

112 2.1.1. Reactives

113 RuCl₃, pyridine derivated ligands and methyl-benzylamines, were purchased from Fluka. KPF₆,
114 NH₄PF₆, salts used for buffer preparation, mobile phases and ubiquitin were commercial products from
115 Sigma-Aldrich. Solvents were purchased from Sigma-Aldrich and Panreac. Ligand dppz was
116 synthesized fromSigma-Aldrich commercial products. PCI was extracted directly from potato.

117

118 2.1.2. Solutions and buffers

119 TE: 10 mM tris-HCl (tris-[hydroxymethyl]aminomethane hydrochloride),

120 0,1 mM EDTA (ethylenediaminetetraacetic acid), 50 mM NaCl; pH was adjusted to 7.4 with NaOH.

121 TBE: 45 mM tris-base (tris-[hydroxymethyl]aminomethane), 45 mM boric acid, 1 mM EDTA
122 (ethylenediaminetetraacetic acid); pH was adjusted to 8 with NaOH. HEPES: 40 mM de HEPES (4-(2-
123 hydroxyethyl)-1-piperazineethane sulfonic acid), 10 mM MgCl₂; pH was adjusted to 7.4 with NaOH

124 Color marker: bromophenol blue (0.25%), xilencianol FF (0.25%), glycerol 25%.

125 PBS: 150mMNaCl, 3mMKCl, 9mMNa₂PO₄, 1.3mMK₂PO₄; pHwas adjusted to 7.2 with NaOH.

126

127 2.1.3. DNA and general materials for DNA experiments

128 DNA calf thymus highly polymerized sodium salt (SIGMA); Plasmid pBR322 0.25 µg/µl (Boehringer
129 Mannheim GmbH); Agarose AG-200 molecular biology grade (ECOGEN); ethidium bromide
130 (MERCK).

131

132 2.1.4. Protein solutions preparation. Proteins: Ubiquitin and potato carboxypeptidase inhibitor (PCI)

133 Ubiquitin 3 mM solution was prepared dissolving commercial lyophilized ubiquitin in mQ water. PCI
134 solution 1.86 mM was prepared dissolving the protein directly extracted from potato, in mQ water.
135 Protein concentration was determined in both cases through absorbance measurements with UV–visible
136 (UV–Vis) spectrophotometer CARY 100 SCAN (Varian) as predicted by Lambert–Beer theory. Molar
137 absorptivity coefficient estimation was made with the method proposed by Grimsley et al. [25].

138

139 2.2. Devices and methods

140

141 2.2.1. X-ray diffraction analysis

142 Crystal structures were registered with an ENRAF-NONIUS CAD4. Software for structure refining was
143 SHELXS97 and SHELXL97. Crystals were obtained through diethyl ether slowdiffusion in saturated
144 dichloromethane solutions of the compounds.

145 2.2.2. Elemental analysis

146 Elemental analysis of (C, H, N, S) was carried out with a CARLO ERBA EA1108.

147

148 2.2.3. Infrared spectroscopy

149 IR spectra between 4000 and 600 cm⁻¹ were registered with a spectrophotometer NICOLET 5700 FT-
150 IR, in solid phase in KBr matrix.

151

152 2.2.4. NMR spectroscopy

153 ¹H, ³¹P{¹H} and ¹⁹F{¹H} NMR were registered in a 300 MHz VARIAN UNITY. Samples were
154 dissolved in CDCl₃.

155

156 2.2.5. Atomic force microscopy (AFM)

157 Atomic force microscopy images were obtained in TMAFM mode with a NANOSCOPE III
158 MULTIMODE AFM from Digital Instruments Inc.

159 Sample preparation: DNA was treated for 15 min at room temperature to obtain a homogeneous
160 topoisomer distribution. Stock solution 1 mg/ml was prepared in a maximum rate DMSO:HEPES 6:4,
161 for non water soluble complexes. It was then diluted 1:1000 in HEPES until a final volume of 2000 μl,
162 and therefore filtered through FP030/3 0.2 nm pore filters (Schleicher & Schuell GmbH). Each sample
163 consists of 1 μl of pBR-322 plasmid DNA (0.25 μg/μl), 2 μl of drug filtered solution and then carried to
164 a final volume of 50 μl with HEPES. Samples were incubated during 5 and 24 h at 37 °C. 2 μl of each
165 sample are adsorbed over a mica disk (Ashville-Schoonmaker Mica Co., Newport News), washed with
166 mQ water and dried under argon or nitrogen.

167

168 2.2.6. Circular dichroism

169 Circular dichroism spectra were registered with a spectropolarimeter JASCO 810, equipped with a
170 450W Xenon arc lamp.

171 Sample preparation: 1 mg/ml stock solutions of each compound were prepared immediately before using
172 in a DMSO:TE sterilized mixture (2% DMSO maximum). 20 μg/ml calf thymus DNA solution was
173 prepared in TE and stored at 4 °C. DNA quantization was verified by UV-Vis spectroscopy, checking
174 absorbance at 260 nm in a split double beam SHIMADZU UV-2101-PC spectrophotometer.
175 Compound-DNA adduct formation was carried out by addition of solution stock aliquots of each
176 compound to a fixed volume of DNA solution. Amount of drug added in each case is expressed as *r_i*
177 (theoretical molar ratio compound-nucleotide) and is calculated as can be seen in the additional
178 information.

179

180
$$r_i = \frac{m \times M_{nucl} \times A_m}{C \times M_r \times V} \cdot r_i^{1/4}$$

181

182 *m* mass of compound used to prepare stock solution (μg)

183 *M_{nucl}* average molecular mass by nucleotide (g/mol)

184	Am	number of metallic atoms in compound
185	C	DNA solution concentration ($\mu\text{g}/\text{ml}$)
186	Mr	molecular mass of each compound (g/mol)
187	V	sample final volume (ml)

188

189 All experiments were carried out for molar ratios of 0.1, 0.3 and 0.5, which means that in each case there
 190 are 1, 3 and 5 molecules of compound respectively versus each ten pairs of DNA nitrogen bases.
 191 Through this formula the μg of compound (or μl of stock solution) that must be added to DNA solution
 192 in each case can be calculated. The sample holder had 5 l/min nitrogen flowpurge. 1 cm path length
 193 quartz cells were used for measurements. Each sample was registered twice in a wavelength interval of
 194 220 and 330 nm, rate of 50 nm/min.

195

196 2.2.7. Agarose gel electrophoresis

197 Electrophoresis experiments were carried out in an ECOGEN horizontal tank connected to a
 198 PHARMACIA GPS 200/400 variable tension source. Gel images were recorded with a thermal system
 199 FUJIFILM FTI-500.

200 Sample preparation: stock solution preparation for each compound was the same to the one described for
 201 circular dichroism. Buffer solution was TE (2% DMSO maximum). Sample final volume was 20 μl : 2.8
 202 μl of DNA pBR322 solution 0.25 $\mu\text{g}/\mu\text{l}$, the volume of stock solution necessary to obtain the
 203 desired molar ratio ($r_i = 0.5$), and filling until 20 μl with TE buffer solution. In this way, the final
 204 concentration of DNA plasmid was 35 $\mu\text{g}/\text{ml}$ so each sample contained 0.7 μg of DNA. After incubation
 205 at 37 °C for 24 h of 20 μl compound-DNA solution samples 4 μl of color marker was added. The
 206 mixture went through electrophoresis in 0.5% agarose gel in TBE buffer at 1.5 V/cm for 4 h. After that
 207 DNA was stained with ethidium bromide solution (0.5 $\mu\text{g}/\text{ml}$ in TBE) during 20 min. Negative control
 208 was a free plasmid pBR322 DNA solution, and for positive control cisplatin-DNA samples in the same
 209 conditions of all other complexes were prepared.

210

211 2.2.8. Molecular fluorescence

212 Fluorescence molecular emission measurements were registered with a spectrofluorimeter Kontron
 213 SFM-25 (Bio-Tek Instruments).

214 Sample preparation: several 3 ml aliquots from a calf thymus DNA 50 μM standard stocking
 215 solution were taken, adding to them necessary amount (30 μl) of ethidium bromide 5 mM to get 1:1 molar
 216 ratio, and they were incubated for 30 min at 37 °C. Afterwards, growing amounts (0, 20, 40, 60, 80 y
 217 100 μl) of compound stock solution (1.5 mM DMSO/mQ water) were added to different samples, to
 218 obtain different complex concentrations in each one (0, 10, 20, 30, 40 y 50 μM respectively). Emission
 219 spectra were registered between 530 and 670 nm and excitation wavelength was established in 502 nm.
 220 DMSO concentration in final samples was always below 2%.

221

222 2.2.9. Viscosity measurements

223 DNA solutions viscosity measurements were carried out with a Vibro Viscometer SV-1^a (AND A&N
 224 Company Limited).

225 Sample preparation: 1ml stock solution 5mM of each compound in DMSO/water (4:1), and 1mM calf
226 thymus DNA solution were prepared. Afterwards, several aliquots of 1 ml from this last were transferred
227 to different sterilized tubes, adding then 3 ml of TE buffer, which corresponds with DNA control
228 solution. For each compound, increasing amounts of stock solution (20, 60 and 100 μ l) were added to
229 reach molar ratios of 0.1, 0.3 and 0.5 DNA: complex, respectively. In all of them viscosity at 25 °C was
230 measured before and after mixing, and along the time as well (0, 4, 14, 32, 44 and 56 h), keeping
231 constant temperature with a thermostated water bath for the samples and isobutyl alcohol bath for
232 viscometer devices. Again, DMSO concentration in biological samples did not exceed 2%.

233

234 2.2.10. Mass spectrometry

235 Matrix-assisted laser desorption ionization-time of flight (MALDI-TOF) mass spectra were obtained
236 with a VOYAGER DE-RP (Applied Biosystems) mass spectrometer provided with a nitrogen laser (337
237 nm, 3 ns pulsed) and applying 20–25 KV as accelerating voltages. Samples were dissolved in suitable
238 matrixes (DHB 2,5- dihydroxybenzoic acid, Sigma-Aldrich, 10 mg/ml acetonitrile/H₂O 1:1 volume
239 (0.1% TFA)).

240 Infusion high resolution electrospray ionization mass spectrometry (ESI-MS) spectra were carried out
241 with a LC/MSD-TOF (Agilent Technologies) mass spectrometer provided with double nebulizer for
242 exact mass determination. (See Table S1 in Supplementary information for experimental condition
243 details).

244 Liquid chromatography mass spectrometry (LC-MS) experiments were performed on a QSTAR Elite
245 System Hybrid Quadrupole-TOF LC/MS/MS (AB Sciex) using an Agilent 1100 G13112B pump, and an
246 Agilent 1200 G1367C automatic sampler provided with a column oven.

247 Potato carboxypeptidase inhibitor (PCI)-complex and ubiquitin complex adducts (where complex = 1.7),
248 were obtained by aqueous solution reaction at neutral pH and temperature of HPLC autosampler (40
249 °C). Aliquots of 300 μ l of PCI and ubiquitin solutions were taken, and it was added with the necessary
250 amount (μ l) of 0.01 M compound stock solution (DMSO/mQ water, 2% maximum DMSO) to obtain 1:1
251 molar ratio. The system was allowed to react and its evolution was studied by HPLC-MS with 10 μ l
252 sample injection per hour, during 24 h. A Nucleosil 120 C18 10 μ m 25 \times 0.45 cm column was used for
253 chromatographic separation using linear gradients of acetonitrile in aqueous solution (A: ammonium
254 acetate 0.01 M, B: acetonitrile 0–100% flux: 1 ml/min–40 min). A 1:10 split post-column was done for
255 on-line coupling to the mass spectrometer. Experimental mass spectrometry conditions are described in
256 the Supplementary information (Table S2).

257

258 2.2.11. Ion mobility mass spectrometry (IMS-MS)

259 IMS-MS experiments were carried out using a SYNAPT G1 HDMS mass spectrometer (Waters,
260 Manchester, UK). Samples were placed on a 384-well plate refrigerated at 15 °C and introduced by
261 automated chip-base nanoelectrospray using a Triversa NanoMate (Advion Bio-Sciences) in positive ion
262 mode. A reduction of the source pumping speed in the backing region (5.81 mbar) of the mass
263 spectrometer was done for optimal ion transmission. (For detailed experimental conditions see
264 Supplementary Table S3) The instrument was calibrated over the m/z range 500–5000 Da using a
265 solution of cesium iodide. MassLynx vs 4.1 SCN 704 software and Driftscope vs 2.1 software were used
266 for data processing. Experimental drift times were transformed into collision cross sections (CCS, Ω) by
267 constructing a calibration curve with proteins of known collision cross-sections. The calibrant lists are
268 given in Table S4 and the calibration curves are shown in Fig. S2. Experimental drift times for these
269 calibrants were recorded using identical instrument conditions than the studied complexes.

270 They were taken 10 μ l of 3 mM ubiquitin solution and 20 μ l of 1.86 mM PCI solution, and it was added
271 with the necessary volume of complex E1 and E2 0.01 M stock solutions to obtain 1:1 molar ratio.
272 Samples were incubated for 24 h at 37 °C. Afterwards they were diluted with 600 μ l of ammonium
273 acetate buffer, and 10 μ l of this diluted solution was poured in the sample plate of the Advion Triversa
274 Nanomate. DMSO concentration never exceeded 2%.

275

276 2.2.12. In vitro cytotoxicity and apoptosis assays on HL-60 cells

277

278 2.2.12.1. Tumor cell lines and culture conditions. The cell line used was the human acute promyelocytic
279 leukemia cell line HL-60 (American Type Culture Collection (ATCC)). Cells were routinely maintained
280 in RPMI-1640 medium supplemented with 10% (v/v) heat inactivated fetal bovine serum, 2 mmol/l
281 glutamine, 100 U/ml penicillin, and 100 μ g/ml streptomycin (Gibco BRL, Invitrogen Corporation,
282 Netherlands) in a highly humidified atmosphere of 95% air with 5% CO₂ at 37 C.

283

284 2.2.12.2. Cytotoxicity assays. Growth inhibitory effect of the ruthenium complexes on the leukemia HL-
285 60 cell line was measured by the microculture tetrazolium, [3-(4,5-dimethylthiazol-2-yl)-2,5-
286 diphenyltetrazolium bromide, MTT] assay [26]. Briefly, cells growing in the logarithmic phase were
287 seeded in 96-well plates (104 cells per well), and then were treated with varying doses of the ruthenium
288 complex and the reference drug cisplatin at 37 C for 24 h. For each of the variants tested, four wells
289 were used. Aliquots of 20 μ l of MTT solution were then added to each well. After 3 h, the color formed
290 was quantified by a spectrophotometric plate reader at 490 nm wavelength. The percentage of cell
291 viability was calculated by dividing the average absorbance of the cells treated with the complex by that
292 of the control; IC₅₀ values (drug concentration at which 50% of the cells are viable relative to the
293 control) were obtained by GraphPad Prism software, version 4.0.

294

295 2.3. Synthesis

296

297 2.3.1. Synthesis of complexes without PPh₃ moiety (see Fig. S1)

298 2.3.1.1. Synthesis of [RuII(Cl)₂(p-cymene)]₂ (1). A suspension of RuCl₃ (0.1 g, 0.36 mmol) in ethanol
299 (40 ml) was heated under reflux during 8 h with 6 equivalents (2 ml, 18 mmol) of R- α -phellandrene,
300 keeping the stirring afterwards during 12 h more at room temperature. Solvent was removed under
301 reduced pressure until an orange precipitate was observed, which was filtered off, washed with cold
302 methanol and dried under reduced pressure.

303 Yield: 65%; M.S.[ESI]: m/z 576.9 {M-Cl}⁺; Anal. Calc. C₂₀H₂₈Cl₄Ru₂: 39.23% C, 4.61% H; Anal.
304 Exp.: 39.39% C, 4.51% H; ¹H NMR [CDCl₃]: δ a 5.48, δ b 5.35 (dd, J(HH) \approx 6.0 Hz, 4H, C_{2,3,5,6}-
305 H{ring}), δ 2.93 (sep, J(HH) \approx 7.0 Hz, H, CH(Me)₂), δ 2.16 (s, 3H, CH₃{ring}), δ 1.28 (d, JHH \approx 7.0
306 Hz, 6H, CH(Me)₂); IR: 3052.68 (ν Csp²-H), 2961.22 (ν Csp³-H), 1468–1386 (ν C-C).

307

308 2.3.1.2. Synthesis of [RuII(Cl)₂(p-cymene)(4-(2-EtOH)Py)] (2). A suspension of (1) (0.1 g, 0.16 mmol)
309 and 4-(2-hydroxyethyl)pyridine (300 μ l, 2.7 mmol) in methanol (30 ml) was heated under reflux during
310 7 h, keeping the stirring afterwards during 12 h more at room temperature. Solvent was removed under
311 reduced pressure until an orange oil was obtained. With the addition of diethyl ether an orange

312 precipitate was obtained, which was filtered off, washed with diethyl ether and dried under reduced
313 pressure.

314 Yield: 83%; M.S.[ESI]: m/z 394.05 {M+Cl}; Anal. Calc. C₁₇H₂₂Cl₂-NORu: 47.56% C, 5.40% H,
315 3.26% N; Anal. Exp.: 47.57 %C, 5.35% H, 3.35% N; ¹H NMR [CDCl₃]: δ 8.88 (d, J(HH) ≈ 6.2 Hz, 2H,
316 C–H{4-(2-EtOH)Py}), δ 7.18 (d, J(HH) ≈ 6.2 Hz, 2H, C–H{4-(2-EtOH)Py}), δ 5.44–5.21 (2d, J(HH) ≈
317 6.0 Hz, 4H, C–H{ring}), δ 3.80 (m, J(HH) ≈ 6.0 Hz, 2H, CH₂{4-(2-EtOH)Py}), δ 3.00 (sep, J(HH) ≈
318 7.0 Hz, H, CH(Me)₂), δ 2.85 (t, J(HH) ≈ 6.0 Hz, 2H, CH₂{4-(2-EtOH)Py}), δ 2.11 (s, 3H, CH₃{ring}),
319 δ 1.31 (d, J(HH) ≈ 7.0 Hz, 6H, CH(Me)₂); IR: 3463.70 (νOH), 816.35 (νRu–N).

320

321 2.3.2. Synthesis of complexes including PPh₃ moiety (see Fig. S1)

322 2.3.2.1. Synthesis of [RuIICl₂(p-cymene)PPh₃] (3). A suspension of (1) (0.55 g, 0.9 mmol) and PPh₃
323 (0.6 g, 2.25 mmol) in hexane (30 ml) was heated under reflux during 5 h, keeping the stirring until it
324 reached room temperature. The red precipitate result was filtered off, washed with hexane and dried
325 under reduced pressure.

326 Yield: 82%; M.S.[ESI]: m/z 586.1 {M-Cl}⁺; Anal. Calc. C₂₈H₂₉Cl₂Ru: 59.16% C, 5.14% H; Anal.
327 Exp.: 58.83% C, 5.04% H; ¹H NMR [CDCl₃]: δ 7.37–7.83 (m, 15H, PPh₃), δ_a 5.18, δ_b 4.99 (2d, J(HH)
328 ≈ 6.0 Hz, 4H, C–H{ring}), δ 2.85 (sep, J(HH) ≈ 7.0 Hz, H, CH(Me)₂), δ 1.87 (s, 3H, CH₃{ring}), δ 1.11
329 (d, J(HH) ≈ 7.0 Hz, 6H, CH(Me)₂); ³¹P{¹H}NMR [CDCl₃]: δ 24.16 (s, PPh₃); IR: 1091.21 (νP–C),
330 520.95 (πC–P–C).

331

332 2.3.2.2. Synthesis of [RuIICl(p-cymene)(3-picoline)PPh₃][PF₆] (4).

333 A suspension of (3) (0.1 g, 0.18 mmol), KPF₆ (0.04 g, 0.2 mmol) and 3-methylpyridine (3-picoline, 400
334 μl, 4.0 mmol) in methanol (30 ml) was stirred during 24 h at room temperature. Solvent was removed
335 under reduced pressure until a yellow oil was obtained. With the addition of diethyl ether a yellow
336 precipitate was obtained, which was filtered off, washed with diethyl ether and dried under reduced
337 pressure.

338 Yield: 78%; M.S.[ESI]: m/z 626.13 {M⁺}; Anal. Calc. C₃₄H₃₆ClF₆NP₂Ru: 52.96% C, 4.71% H, 1.82%
339 N; Anal. Exp.: 53.13% C, 4.83, 1.82% N; ¹H NMR [CDCl₃]: δ 8.76 (d, J(HH) ≈ 5.0 Hz, H, C–H{3-
340 picoline}), δ 8.53 (s, H, C–H{3-picoline}), δ 7.27–7.57 (m, 16H, PPh₃, 3-picoline), δ 7.04 (d, J(HH) ≈
341 2.0 Hz, H, C–H{3-picoline}), δ 5.95–5.30 (4d, J(HH) ≈ 5.0 Hz, 4H, C–H{ring}), δ 2.18 (sep, J(HH) ≈
342 6.4 Hz, H, CH(Me)₂), δ 2.12 (s, 3H, CH₃{3-picoline}), δ 1.65 (s, 3H, CH₃{ring}), δ 1.10 (2d, J(HH) ≈
343 7.0 Hz, 6H, CH(Me)₂); ³¹P{¹H}NMR [CDCl₃]: δ 37.3 (s, PPh₃), δ –144.1 (sep, J(PF) ≈ 713 Hz, PF₆
344 –), ¹⁹F{¹H}NMR [CDCl₃]: δ –73 (d, J(FP) ≈ 713 Hz, PF₆ –); IR: 1093.02 (νP–C), 840.39 (νRu–N),
345 700.75 (νP–F).

346

347 2.3.2.3. Synthesis of [RuIICl(p-cymene)(3,4-lutidine)PPh₃][PF₆] (5). A suspension of (3) (0.1 g, 0.18
348 mmol), KPF₆ (0.04 g, 0.2 mmol) and 3,4-dimethylpyridine (3,4-lutidine, 200 μl, 1.8 mmol) in methanol
349 (30 ml) was heated under reflux during 7 h, keeping the stirring afterwards during 12 h more at room
350 temperature. Solvent was removed under reduced pressure until an orange oil was obtained. With the
351 addition of diethyl ether an orange precipitate was obtained, which was filtered off, washed with diethyl
352 ether and dried under reduced pressure.

353 Yield: 84%; M.S.[ESI]: m/z 640.15 {M⁺}; Anal. Calc. C₃₅H₃₈ClF₆NP₂Ru-H₂O: 52.34 %C, 5.02% H,
354 1.74% N; Anal. Exp.: 52.39% C, 4.60% H, 1.84% N; ¹H NMR [CDCl₃]: δ 8.60 (d, J(HH) ≈ 5.3 Hz, H,

355 C-H{3,5-lutidine}), δ 8.35 (s, H, C-H{3,5-lutidine}), δ 7.26–7.5 (m, 15H, PPh₃), δ 6.90 (d, J(HH) \approx 5.3
356 Hz, H, C-H{3,5-lutidine}), δ 5.98–5.28 (4d, J(HH) \approx 5.7 Hz, 4H, C-H{ring}), δ 2.21 (sep, J(HH) \approx 7.0
357 Hz, H, CH(Me)₂), δ 2.15 (s, 3H, CH₃{3,5-lutidine}), δ 1.99 (s, 3H, CH₃{3,5-lutidine}), δ 1.64 (s, 3H,
358 CH₃{ring}), δ 1.11 (2d, J(HH) \approx 5.0 Hz, 6H, CH(Me)₂); ³¹P{¹H}NMR [CDCl₃]: δ 37.7 (s, PPh₃), δ
359 –144.1 (sep, J(PF) \approx 713 Hz, PF₆[–]), ¹⁹F{¹H} NMR [CDCl₃]: δ –73 (d, J(FP) \approx 713 Hz, PF₆[–]); IR:
360 1092.35 (vP–C), 840.39 (vRu–N), 700.30 (vP–F).

361

362 2.3.2.4. Synthesis of [RuII(Cl)(p-cymene)(3,5-lutidine)PPh₃][PF₆] (6). A suspension of (3) (0.1 g, 0.18
363 mmol), KPF₆ (0.04 g, 0.2 mmol) and 3,5-dimethylpyridine (3,5-lutidine, 200 μ l, 1.8 mmol) in methanol
364 (30 ml) was heated under reflux during 7 h, keeping the stirring afterwards during 12 h more at room
365 temperature. Solvent was removed under reduced pressure until an orange oil was obtained. With the
366 addition of diethyl ether an orange precipitate was obtained, which was filtered off, washed with diethyl
367 ether and dried under reduced pressure.

368 Yield: 89%; M.S.[ESI]: m/z 640.15 {M⁺}; Anal. Calc. C₃₅H₃₈ClF₆NP₂- Ru-H₂O: 52.34% C, 5.02%
369 H, 1.74% N; Anal. Exp.: 52.61% C, 4.72% H, 1.89% N; ¹H NMR [CDCl₃]: δ 8.43 (s, 2H, C-H{3,5-
370 lutidine}), δ 7.27–7.50 (m, 15H, PPh₃), δ 7.11 (s, H, C-H{3,5-lutidine}), δ 5.99–5.35 (4d, J(HH) \approx 5.4
371 Hz, 4H, C-H{ring}), δ 2.20 (sep, J(HH) \approx 7.0 Hz, H, CH(Me)₂), δ 2.11 (s, 6H, 2CH₃{3,5-lutidine}), δ
372 1.64 (s, 3H, CH₃{ring}), δ 1.11 (2d, J(HH) \approx 7.5 Hz, 6H, CH(Me)₂); ³¹P{¹H}NMR [CDCl₃]: δ 38.1 (s,
373 PPh₃), δ –144.1 (sep, J(PF) \approx 713 Hz, PF₆[–]), ¹⁹F{¹H}NMR [CDCl₃]: δ –73 (d, J(FP) \approx 713 Hz, PF₆
374 –); IR: 1092.65 (vP–C), 836.70 (vRu–N), 700.41 (vP–F).

375

376 2.3.2.5. Synthesis of [RuII(Cl)(p-cymene)(4-(2-EtOH))PPh₃][PF₆] (7). A suspension of (3) (0.1 g, 0.18
377 mmol), NH₄PF₆ (0.03 g, 0.2 mmol) and 4-(2-hydroxyethyl)pyridine (300 μ l, 2.7 mmol) in methanol (30
378 ml) was heated under reflux during 7 h, keeping the stirring afterwards during 12 h more at room
379 temperature. Solvent was removed under reduced pressure until a yellow oil was obtained. After the
380 addition of some drops of DMSO, a brown precipitate was obtained with the addition of H₂O. The
381 precipitate obtained was filtered off, washed with deionized water and dried under reduced pressure.

382 Yield: 69%; M.S.[ESI]: m/z 656.14 {M⁺}; Anal. Calc. C₃₅H₃₈ClF₆NOP₂- Ru-NH₄: 48.67% C, 4.74%
383 H, 3.66% N; Anal. Exp.: 49.16% C, 4.66%, 3.57% N; ¹H NMR [CDCl₃]: δ 8.73 (d, J(HH) \approx 6.3 Hz,
384 2H, C-H{4-(2-EtOH)Py}), δ 7.27–7.50 (m, 15H, PPh₃), δ 7.02 (d, J(HH) \approx 6.3 Hz, 2H, C-H{4-(2-
385 EtOH)Py}), δ 5.93–5.25 (4d, J(HH) \approx 6.0 Hz, 4H, C-H{ring}), δ 3.77 (m, J(HH) \approx 7.0 Hz, 2H, CH₂{4-
386 (2-EtOH)Py}), δ 2.76 (t, J(HH) \approx 6.0 Hz, 2H, CH₂{4-(2-EtOH)Py}), δ 2.24 (sep, J(HH) \approx 7.0 Hz, H,
387 CH(Me)₂), δ 1.66 (s, 3H, CH₃{ring}), δ 1.10 (d, J(HH) \approx 7.0 Hz, 6H, CH(Me)₂); ³¹P{¹H}NMR
388 [CDCl₃]: δ 37.1 (s, PPh₃), δ –144.1 (sep, J(PF) \approx 713 Hz, PF₆[–]), ¹⁹F{¹H}NMR [CDCl₃]: δ –73 (d,
389 J(FP) \approx 713 Hz, PF₆[–]); IR: 3533.84 (vOH), 1093.69 (vP–C), 840.42 (vRu–N), 700.86 (vP–F).

390

391 2.3.2.6. Synthesis of [RuII(Cl)(p-cymene)(PPh₃)₂][PF₆] (8). A suspension of (3) (0.1 g, 0.18 mmol),
392 KPF₆ (0.04 g, 0.2 mmol) and PPh₃ (0.1 g, 0.4 mmol) in methanol (30 ml) was stirred during 2 h at 35
393 °C. Solvent was removed at room temperature under reduced pressure until a yellow oil was obtained.
394 With the addition of hexane a yellow precipitate was obtained, which was filtered off, washed with
395 ethanol/hexane 1:2 and dried under reduced pressure.

396 Yield: 78%; M.S.[ESI]: m/z 795.16 {M⁺}; Anal. Calc. C₄₆H₄₄ClF₆P₃Ru: 58.76% C, 4.72% H; Anal.
397 Exp.: 58.56% C, 4.79% H; ¹H NMR [CDCl₃]: δ 7.45–7.22 (m, 30H, 2PPh₃), δ 5.60–5.00 (2d, J(HH) \approx
398 6.4 Hz, 4H, C-H{ring}), δ 2.70 (sep, J(HH) \approx 7.0 Hz, H, CH(Me)₂), δ 1.22 (d, J(HH) \approx 7.0 Hz, 6H,
399 CH(Me)₂), δ 1.10 (s, 3H, CH₃{ring}); ³¹P{¹H}NMR [CDCl₃]: δ 20.67 (s, PPh₃), δ –144.1 (sep, J(PF)

400 ≈ 713 Hz, PF6 $-$), ^{19}F $\{^1\text{H}\}$ NMR [CDCl_3]: $\delta -73$ (d, $J(\text{FP}) \approx 713$ Hz, PF6 $-$); IR: 1089.04 ($\nu\text{P-C}$),
401 831.44 ($\nu\text{Ru-N}$), 699.03 ($\nu\text{P-F}$), 516.46 ($\pi\text{C-P-C}$).

402

403 2.4. Crystallographic analysis

404

405 Single crystal X-ray diffraction experiments were carried out with suitable selected crystals of
406 (2),(4),(5),(6) and (7), mounted at the tip of a glass fiber on an ENRAF-NONIUS CAD4 producing
407 graphite monochromatic Mo $\text{K}\alpha$ radiation ($\lambda = 0.71073$ Å). The structures were solved using the
408 WINGX package. A summary of the crystal data can be seen in Table 1. Core length and refinements
409 parameters are included in the Supplementary information (Tables S5). Images of each one of the
410 complexes analyzed can be seen in Figs. 2–6. CCDC 857319–857323 contain the Supplementary
411 crystallographic data for this paper. These data can be obtained free of charge from the Cambridge
412 Crystallographic Data Centre via www.ccdc.cam.ac.uk/data_request/cif.

413

414 3. RESULTS AND DISCUSSION

415

416 3.1. DNA interaction studies

417

418 3.1.1. Circular dichroism

419 The circular dichroism spectrum of calf-thymus DNA in TE buffer shows a negative band with $\lambda_{\max} =$
420 46 nm and a positive band with $\lambda_{\max} = 275$ nm, characteristics of right-handed B-form DNA [27].

421 Although most of the induced changes in CD spectrum not very significant (with notable negative and
422 positive bands intensity decrease), complex (2) and complex (8) caused important changes in ellipticity
423 of calf thymus DNA and so distortion of its secondary structure (Fig. 7).

424

425 3.1.2. Agarose gel electrophoresis

426 Calf thymus DNA contains two main conformational topoisomers, open circular (OC) and covalently
427 closed circular (CCC). Agarose gel electrophoresis studies can show the distortion of tertiary structure
428 due to the interaction between drugs and DNA. The image in Fig. 8 shows calf thymus DNA migration
429 through agarose gel for untreated DNA and several DNA-metallic complex adducts.

430 As seen below any of these complexes distorts DNA tertiary structure in a way able to change the
431 topoisomer's distribution pattern. Only DNA-cisplatin adducts show the typical coalescence of both CC
432 and CCC signals due to the formation of cis covalent bonding adducts.

433 These results suggest that the interaction between DNA and current ruthenium complexes could be
434 different from the one established between DNA and cisplatin. It is well known that DNA-cisplatin
435 adducts are preferentially intrastand cis covalent binding, so it can be concluded that current ruthenium
436 complexes must bind DNA in a different way, since its effect in DNA agarose gel electrophoresis
437 migration is completely different.

438

439 3.1.3. Molecular fluorescence

440 Based on previous results, ethidium bromide quenching studies were carried out to elucidate whether π -
441 stacking bonding could have any contribution to DNA ruthenium complex interaction or not. Ethidium
442 bromide is a typical intercalator that can bond DNA nitrogen bases intercalating between them.

443 Ethidium bromide displacement studies are one of the most simple and potent tools to find out if any
444 compound can bind DNA nitrogen bases through π -stacking interaction [28].

445 Images on Fig. 9 show the molecular fluorescence spectra of DNA-cisplatin (negative control), DNA-9-
446 acridine (positive control) and DNA-ruthenium complex 2 and 8 adducts. As seen below, for positive
447 control decrease intensity of molecular fluorescence occurs when increasing drug ratio due to the
448 consequent higher ethidium bromide displacement, and so increasing fluorescence quenching. On the
449 other hand, negative control, shows no molecular fluorescence signal variation, as expected for
450 compounds that are not able to stand π -stacking interactions with DNA nitrogen bases. See additional
451 spectra for all compounds in the Supplementary information (Fig. S4).

452 These plots showed intensity decrease pattern for all the ruthenium complexes except for complex 2, the
453 only one lacking PPh₃ moiety in its structure. Different amounts of decrease was found for each one of
454 them, achieving highest quenching values for complex 8, since it includes two PPh₃ groups in its

455 structure. These results suggest that PPh₃ presence could induce intercalation between nitrogen bases
456 through π -stacking based interactions.

457

458 3.1.4. Viscosity measurements

459 Optical photophysical probes provide necessary, but not sufficient clues to support a binding model.
460 Hydrodynamic measurements (i.e., viscosity and sedimentation) that are sensitive to length change are
461 regarded as the least ambiguous and the most critical tests of a binding model in solution in absence of
462 crystallographic structural data [29]. A classical intercalation model results in lengthening the DNA
463 helix as base pairs are separated to accommodate the bound ligand, leading to the increase of DNA
464 viscosity. In contrast, non-intercalative model, could bend or kink the DNA helix, reduce its effective
465 length, and concomitantly, its viscosity. In addition, electrostatic or minor groove binding (capable of
466 EtBr quenching in some occasions) has no influence on DNA viscosity [30]. Fig. 10 shows the change
467 in viscosity of several calf thymus DNA solutions in TE when treated with increasing ratios of
468 ruthenium complexes.

469 As seen in Fig. 10 all complexes cause an important increase in DNA solutions viscosity when
470 increasing its concentration, except the only one lacking PPh₃ moiety in its structure. This phenomenon
471 confirms the intercalative model induced by PPh₃ plane rings, probably in combination with pyridine
472 derivate ring as a π -stacking sandwich system. In addition, higher increase in viscosity takes place for
473 complex 8, again, the one with more PPh₃ moieties included in its structure.

474

475 3.1.5. Atomic force microscopy

476 Ruthenium complex interaction with pBR322 DNA in HEPES buffer solution was studied by atomic
477 force microscopy (AFM). The results obtained are depicted in Fig. 11. As can be seen, ruthenium
478 complex binding causes DNA chain aggregation (complex 2), DNA chain opening (complex 6), kinks
479 (complexes 6, 7), cross-linking and supercoiling (complexes 4–7, remarkably complex 5), and even
480 chain fracture (complexes 5, 6), showing very different DNA morphologies related to untreated DNA.

481 Once more, pBR322-complex 2 system shows different topoisomer morphologies compared to the rest
482 of ruthenium complexes, which is consistent with the intercalation binding model proposed for all of
483 them except for complex 2.

484

485 3.2. Protein interaction studies

486

487 Although DNA is considered as the primary target for most of the metallo-drugs studied so far [31], this
488 belief is based mainly on studies carried out for platinum based anticancer compounds [32]. However,
489 mechanism of action of ruthenium-based anticancer compounds is comparatively unexplored, although
490 it is clear that ruthenium compounds interact more weakly with DNA relative to platinum complexes
491 [33]. There is evidence suggesting that ruthenium compounds might directly interfere with specific
492 proteins involved in signal transduction pathways and/or alter cell adhesion and transduction processes
493 [34–36]. With this frame, ruthenium complex reactivity studies in the presence of model and specific
494 proteins (ubiquitin and potato carboxypeptidase inhibitor-PCI respectively) have been carried out.

495 Ubiquitin is a model protein that plays many different roles in metabolism, and it is ubiquitous in the
496 organism. On the other hand, PCI is a specific protein that can act as an antagonist of human epidermal
497 growth factors (EGF) which are over expressed in tumor cells [37,38]. In fact, PCI is considered as a

498 cytostatic agent, able to block the cell cycle between G0 and G1 phases selectively in cancer cells,
499 without directly inducing apoptosis [39]. All these phenomena suggest the capability of PCI to
500 vehiculize ruthenium metallo-drugs in a selective way to tumor cells (see structures of both proteins in
501 Fig. S5 in the Supplementary information).

502

503 3.2.1. HPLC–MS ruthenium complex–protein interaction study

504 High-resolution ESI MS has been known as a potent tool to study covalent and non-covalent ligand–
505 biomolecule interactions [40–42] and to screen complex mixtures of metabolites, often without the need
506 for chromatographic separation of the adducts prior to analysis [43–45]. In this case, HPLC–MS studies
507 allowed to evaluate the interaction of ruthenium complexes with both model and specific proteins, as
508 well as to elucidate the implications of the presence of PPh3 moiety in this interaction.

509 Graphics on Figs. 12 and 13 show a summary of the decrease of free protein signal while increasing
510 ruthenium complex–protein adduct solution content within the time (see all complete mass spectra in the
511 Supporting information, Fig. S6).

512 In the case of PCI protein (Fig. 12), when PPh3 ligand is present the kinetics of the reactions is very
513 influenced, taking more time to detect the PCI-ruthenium complex adduct and in smaller quantities. On
514 the other hand, when no PPh3 moiety is present, almost all the free protein content disappears in very
515 short period of time, to be mainly in PCIruthenium complex adduct form.

516 Added to that, for ubiquitin protein (Fig. 13), it was not possible to detect the presence of ubi-ruthenium
517 complex adduct when PPh3 ligand was present. All that data suggest that the PPh3 presence affects in a
518 very important manner to the adduct formation process kinetics, which could have very important
519 consequences in the detoxification processes and/or in the delivery of these drugs and cell uptake,
520 allowing slower pharmacokinetics (which usually means less secondary effects) and higher resistance to
521 drug removal in natural detoxification processes.

522

523 3.2.2. IMMS — Ion mobility mass spectrometry studies

524 Ion mobility mass spectrometry can provide information on the physical size and shape of ionized
525 molecules [46] and previous works on related Ru-based complexes have demonstrated the use of this
526 technique for the separation of geometrical isomers and the calculation of their collision cross-sections
527 (CCSs) [47].

528 In this technique, basically, a liquid sample is ionized and injected into a drift chamber containing
529 neutral gas at a controlled pressure (e.g., 0.5 mbar of nitrogen gas). Under the influence of an electric
530 field, gaseous ions undergo IM separation according to the resistance they experience through their
531 collision with neutrals, which depends on their collision cross section-to-charge ratio (Ω/z). After
532 separation, ions are sampled by a mass spectrometer and analyzed according to their mass-to-charge
533 (m/z) ratio. Therefore, integrated IMS–MS has the capability of separating ions not only by their mass
534 but also by their size, shape and charge state. IM–MS offers an extra degree of analytical opportunity
535 whereby conformational ensembles of species of equivalent mass, or the same m/z , can be separated on
536 account of their physical shape and then mass analyzed in a single, rapid experiment. The experimental
537 drift times (arrival times) can be correlated to collision cross sections by performing calibration curves
538 with protein standards of known cross sections analyzed under identical instrumental conditions.
539 Significant changes in CCS should be evaluated as they reflect conformational changes that could affect
540 some functions of the protein. More detailed information about IMS–MS can be found in the literature
541 [48].

542 As mentioned before, PCI protein can act as a vehicle for anticancer drugs towards specific cancer cells
543 in case the binding of the metal complexes doesn't distort the protein structure, since it is an antagonist
544 of EGFs. With the aim of studying the conformational changes of PCI and ubiquitin due to the ruthenium
545 complexes binding IMS–MS experiments were carried out.

546 MS spectra shown in Fig. 14 demonstrate the binding of different fragments of ruthenium complexes to
547 both PCI and ubiquitin, and reinforce previous conclusions out of HPLC–MS studies. As can be seen,
548 again, the presence of PPh3 moiety affords slower kinetics and smaller yields of protein–metal complex
549 binding, which should have important consequences in terms of drug distribution and detoxification
550 mechanisms.

551 Table 2 shows the CCSs obtained when relating the drift times out of the IMS–MS experiments for each
552 molecule reaching the detector, with the cross section calibration curve made with protein standards (see
553 also Fig. S2 in the Supplementary information).

554 As shown in the table, the differences in CCS upon ligand interaction with UBI and PCI lay between
555 0.02 and 11.7% which suggests no significant conformational changes in the three-dimensional gas-
556 phase protein structure. That would support both the possibility of drug delivery by model proteins as
557 ubiquitin and the possibility of specific vehiculization towards cancer cells by specific proteins as PCI.

558

559 3.3. Cytotoxicity studies

560

561 Cytotoxicity studies were carried out for complexes 2–7 in HL60 Human Leukemia Tumor Cell Line,
562 affording IC50 values shown in Table 3.

563 The cytotoxic properties of the complexes including PPh3 ligand in its structure correspond to values
564 comparable to the cytotoxicity obtained for cis-platin and ruthenium complexes active against cancer
565 cell lines in similar experiments [49] (notice that ruthenium complexes undergo some special processes,
566 such as hydrolysis and different bindings compared to cis-platin), while the only one that lack this
567 moiety raises over 200 μM , so it cannot be considered an active drug towards this type of tumor cell
568 line.

569 These results added to the fact that previous investigations carried out in our group [50] in which most
570 of the complexes studied in the present work, but lacking PPh3 moiety, were evaluated as antitumor
571 drugs showing poor antiproliferative properties, strongly suggest an important increment of the
572 antitumor properties of ruthenium complexes due to PPh3 presence.

573

574 **4. CONCLUSIONS**

575

576 Several new organometallic ruthenium complexes, some of them including PPh₃ ligands, have been
577 synthesized and characterized. DNA interaction studies have demonstrated the capability of these
578 complexes to bind DNA and distort its secondary and tertiary structure notably. Ethidium bromide
579 displacement experiments and viscosity measurements prove that those complexes including PPh₃
580 moiety in its structure are able to intercalate into DNA base pairs, whereas those without PPh₃ ligand
581 bind DNA only in a covalent manner. Protein interaction studies have shown the capability of these
582 complexes to bind as well as to model and specific proteins, demonstrating slower kinetics and smaller
583 binding yields when PPh₃ group is present, presumably due to steric impediments. These effects could
584 have important consequences in drug cell up-taken and/or detoxification mechanisms. Finally,
585 cytotoxicity studies show that IC₅₀ values in the range of the ones obtained for cis-platin, considered a
586 positive control for antiproliferative tumor cell studies, in all cases except for the complex lacking PPh₃
587 ligand. That result proves definitively the increment of ruthenium complex antiproliferative potential
588 due to the PPh₃ presence, presumably owing to its capability to intercalate between DNA base pairs.
589 Therefore IMMS studies demonstrate no change in conformational structure of the proteins due to
590 ruthenium complex binding which supports a possible role of PCI as a vehiculizing agent to specific
591 tumor cells for ruthenium complexes.

592

593 **ACKNOWLEDGMENTS**

594

595 Financial support from the Spanish Ministry of “Ciencia e Innovación”, contracts CTQ2008-02064 and
596 BIO2010-22321-C02-01 is kindly acknowledged.

597

598 **REFERENCES**

599

- 600 [1] G. Süss-Fink, *Dalton Trans.* 39 (2010) 1673–1688.
- 601 [2] V. Brabec, O. Nováková, *Drug Resist. Update* 9 (2006) 111–122.
- 602 [3] W.J. Zeller, S. Fruhauf, G. Cheng, B.K. Keppler, E. Frei, M. Kaufmann, *Eur. J. Cancer* 27
603 (1991) 62–67.
- 604 [4] M. Coluccia, G. Sava, F. Loseto, A. Nassi, A. Boccarelli, D. Giordano, E. Alessio, G. Mestroni,
605 *Eur. J. Cancer* 29A (1993) 1873–1879.
- 606 [5] M.J. Clarke, *Coord. Chem. Rev.* 236 (2003) 209–233.
- 607 [6] E. Alessio, G. Mestroni, A. Bergamo, G. Sava, *Curr. Top. Med. Chem.* 4 (2004) 1525–1535.
- 608 [7] Y.K. Yan, M. Melchart, A. Habtemariam, P.J. Sadler, *Chem. Commun.* (2005) 4764–4776.
- 609 [8] A.D. Phillips, O. Zava, R. Scopelitti, A.A. Nazarov, P.J. Dyson, *Organometallics* 29 (2010)
610 417–427.
- 611 [9] P.C.A. Bruijninx, P.J. Sadler, *Adv. Inorg. Chem.* 61 (2009) 1–62.
- 612 [10] A.F.A. Peacock, P.J. Sadler, *Chem. Asian. J.* 3 (2008) 1890–1899.
- 613 [11] S.J. Dougan, P.J. Sadler, *Chimia* 61 (2007) 704–715.
- 614 [12] L. Ronconi, P.J. Sadler, *Coord. Chem. Rev.* 251 (2007) 1633.
- 615 [13] E. Aird, J. Cummings, A.A. Ritchie, M. Muir, R.E. Morris, H. Chen, P.J. Sadler, D.I. Jodrell,
616 *Br. J. Cancer* 86 (2002) 1652.
- 617 [14] R.E. Morris, R.E. Aird, P.D. Murdoch, H.M. Chen, J. Cummings, N.D. Hughes, S. Parsons, A.
618 Parkin, G. Boyd, D.I. Jodrell, P.J. Sadler, *J. Med. Chem.* 44 (2001) 3616.
- 619 [15] R. Fernandez, M. Melchart, E. Vand Der Geer, F. Wang, A. Habtemariam, P.J. Sadler, *J. Inorg.*
620 *Biochem.* 96 (2003) 130.
- 621 [16] F. Wang, H. Chen, J.A. Parkinson, P.D. Murdoch, P.J. Sadler, *Inorg. Chem.* 41 (2002) 4509.
- 622 [17] R. Fernandez, M. Melchart, A. Habtemariam, S. Parsons, P.J. Sadler, *Chem. Eur. J.* 10 (2004)
623 5173.
- 624 [18] M. Melchart, A. Habtemariam, S. Parsons, P.J. Sadler, *J. Inorg. Biochem.* 101 (2007) 1903.

- 625 [19] G. Sava, S. Pacor, M. Coluccia, M. Mariggio, M. Cocchietto, E. Alessio, G. Mestroni, *Drug*
626 *Invest.* 8 (1994) 150.
- 627 [20] O. Novakova, J. Kasparikova, O. Vrana, P.M. van Vliet, J. Reedijk, V. Brabec, *Biochemistry* 34
628 (1995) 12369.
- 629 [21] M.J. Clarke, F. Zhu, D.R. Frasca, *Chem. Rev.* 99 (1999) 2511.
- 630 [22] W.H. Hang, P.J. Dyson, *Eur. J. Inorg. Chem.* (2006) 4003–4018.
- 631 [23] I. Khailaila, A. Bergamo, F. Bussy, G. Sava, P.J. Dyson, *Int. J. Oncol.* 29 (2006) 261–268.
- 632 [24] C.S. Allardyce, P.J. Dyson, F.R. Abou-Shakra, H. Birtwistle, J. Coffey, *Chem. Commun.* (2001)
633 2708–2709.
- 634 [25] C.N. Pace, F. Vajdos, L. Fee, G. Grimsley, T. Gray, *Protein Sci.* 4 (1995) 2411–2423.
- 635 [26] T. Mosmann, *J. Immunol. Methods* 65 (1983) 55–63.
- 636 [27] N. Butenko, A.I. Tomaz, O. Nouri, E. Escibano, V. Moreno, S. Gama, V. Ribeiro, J.P. Telo,
637 J.C. Pessoa, I. Cavaco, *J. Inorg. Biochem.* 103 (2009) 622–632.
- 638 [28] G. Zhang, J. Guo, J. Pan, X. Chen, J. Wang, *J. Mol. Struct.* 923 (2009) 114–119.
- 639 [29] J. Sun, S. Wu, Y. An, J. Liu, F. Gao, L.-N. Ji, Z.-W. Mao, *Polyhedron* 27 (2008) 2845–2850.
- 640 [30] J.G. Liu, B.H. Ye, H. Li, Q.X. Zhen, L.N. Ji, Y.H. Fu, *J. Inorg. Biochem.* 76 (1999) 265.
- 641 [31] V. Brabec, *Prog. Nucleic Acid Res. Mol. Biol.* 71 (2002) 1–68.
- 642 [32] B. Lippert, *Cisplatin: Chemistry and Biochemistry of a Leading Anticancer Drug*, Wiley, New
643 York, 1999.
- 644 [33] G. Pintus, B. Tadolini, A.M. Possadino, B. Sanna, M. Debidda, F. Bennardini, G. Sava, C.
645 Ventura, *Eur. J. Biochem.* 269 (2002) 5861–5870.
- 646 [34] A. Bergamo, A. Masi, P.J. Dyson, G. Sava, *Int. J. Oncol.* 33 (2008) 1281–1289.
- 647 [35] S. Chatterjee, S. Kundu, A. Bhattacharyya, C.G. Hartinger, P.J. Dyson, *J. Biol. Inorg. Chem.* 13
648 (2008) 1149–1155.
- 649 [36] C. Gaiddon, P. Jeannequin, P. Bischoff, M. Pfeffer, C. Sirlin, J.P. Loeffler, *J. Pharmacol. Exp.*
650 *Ther.* 315 (2005) 1403–1411.
- 651 [37] C. Blanco-Aparicio, M.A. Molina, S. Fernández-Salas, M.L. Frazier, J.M. Mas, E. Querol, F.X.
652 Avilés, R. de Llorens, *J. Biol. Chem.* 273 (1998) 12370–12377.

- 653 [38] J.M. Mas, P. Aloy, M. Martí-Renom, B. Oliva, C. Blanco-Aparicio, M.A. Molina, R. de Llorens,
654 E. Querol, F.X. Avilés, *J. Mol. Biol.* 284 (1998) 541–548.
- 655 [39] A. Martínez, V. Moreno, L. Sanglas, R. de Llorens, F.X. Avilés, J. Lorenzo, *Bioorg. Med.*
656 *Chem.* 16 (2008) 6832–6840.
- 657 [40] A. Casini, G. Mastrobuoni, C. Temperini, C. Gabbiani, S. Francese, G. Moneti, C.T. Supuran,
658 A. Scozzafava, L. Messori, *Chem. Commun.* (2006) 156–158.
- 659 [41] C.G. Hartinger, A. Casini, C. Duhot, Y.O. Tsybin, L. Messori, P.J. Dyson, *J. Inorg. Biochem.*
660 102 (2008) 2136–2141.
- 661 [42] A. Casini, C. Gabbiani, E. Michelucci, G. Pieraccini, G. Moneti, P.J. Dyson, L. Messori, *J. Biol.*
662 *Inorg. Chem.* 14 (2009) 761–770.
- 663 [43] R. Breitling, A.R. Pitt, M.P. Barret, *Trends Biotechnol.* 24 (2006) 543–548.
- 664 [44] G. Madalinski, E. Godat, S. Alves, D. Lesage, E. Genin, P. Levi, J. Labarre, J.C. Tabet, E. Ezan,
665 C. Junot, *Anal. Chem.* 80 (2008) 3291–3303.
- 666 [45] J.C. Erve, W. Demaio, R.E. Talaat, *Rapid Commun. Mass Spectrom.* 22 (19) (2008) 3015–3026.
- 667 [46] J.P. Williams, J.A. Lough, I. Campuzano, K. Richardson, P.J. Sadler, *Rapid Commun. Mass*
668 *Spectrom.* 23 (2009) 3563–3569.
- 669 [47] J.P. Williams, T. Bugarcica, A. Habtemariam, K. Giles, I. Campuzano, M. Rodger, P.J. Sadler,
670 *J. Am. Soc. Mass Spectrom.* 20 (2009) 1119.
- 671 [48] B.T. Ruotolo, J.L.P. Benesch, A.M. Sandercock, S.J. Hyung, C.V. Robinson, *Nat. Protoc.* 3 (7)
672 (2008) 1139.
- 673 [49] V. Moreno, J. Lorenzo, F.X. Aviles, M.H. Garcia, J.P. Ribeiro, T.S. Morais, P. Florindo, M. P.
674 Robalo, *Bioinorg. Chem. Appl.* (2010) 936834.
- 675 [50] J. Grau, V. Noe, C. Ciudad, M.J. Prieto, M. Font-Bardía, T. Calvet, V. Moreno, *J. Inorg.*
676 *Biochem.* 109 (2012) 72–81.
- 677 .

678 **Legends to figures**

679

680 **Figure 1** Organometallic ruthenium(II) complex structure.

681

682 **Figure 2.** ORTEP representation of crystallographic structure of complex 2.

683

684 **Figure 3** ORTEP representation of crystallographic structure of complex 4.

685

686 **Fig. 4** ORTEP representation of crystallographic structure of complex 5.

687

688 **Figure 5.** ORTEP representation of crystallographic structure of complex 6.

689

690 **Figure 6.** ORTEP representation of crystallographic structure of complex 7.

691

692 **Figure 7.** CD spectra of DNA–cisplatin and DNA–complex 8 adducts.

693

694 **Fig. 8.** Agarose gel electrophoresis image of untreated DNA (1), DNA-rutheniumcomplex 2, 4–8 (2, 3–
695 7), and DNA–cisplatin (8) adducts.

696

697 **Fig. 9.** Fluorescence emission spectra of DNA-EtBr system treated with some compounds showing
698 different performances depending on the presence of PPh₃ moiety.

699

700 **Fig. 10.** Viscosity evolution for calf thymus DNA solutions treated with synthesized ruthenium
701 complexes.

702

703 **Fig. 11.** Atomic force microscopy (AFM) images of pBR322-DNA plasmid solutions treated with
704 synthesized ruthenium complexes.

705

706 **Fig. 12.** HPLC–MS tuned spectra of PCI-complex 2, 7 solution. Go to Supplementary information Fig.
707 S6 to see all complete mass spectra.

708

709 **Fig. 13.** HPLC–MS tuned spectra of Ubi-complex 2 solution. Go to Supplementary information Fig. S6
710 to see all complete mass spectra.

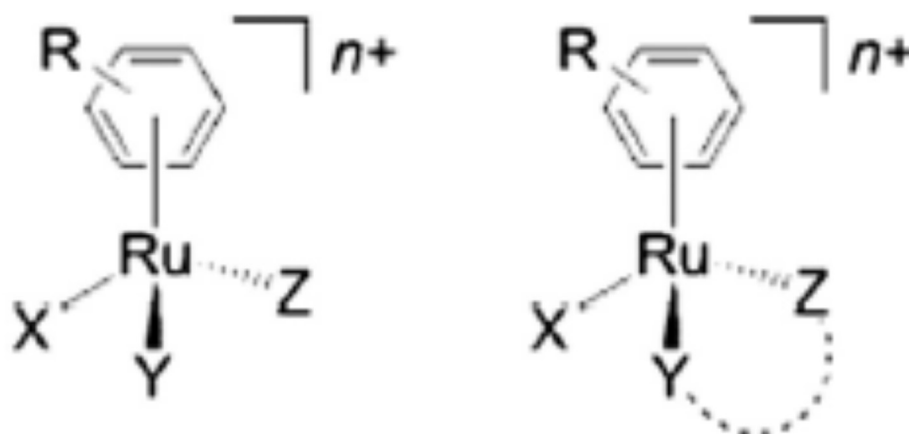
711

712 **Fig. 14.** MS spectra of PCI, UBI, complex 2 and complex 7 combination solutions.

713

714
715
716

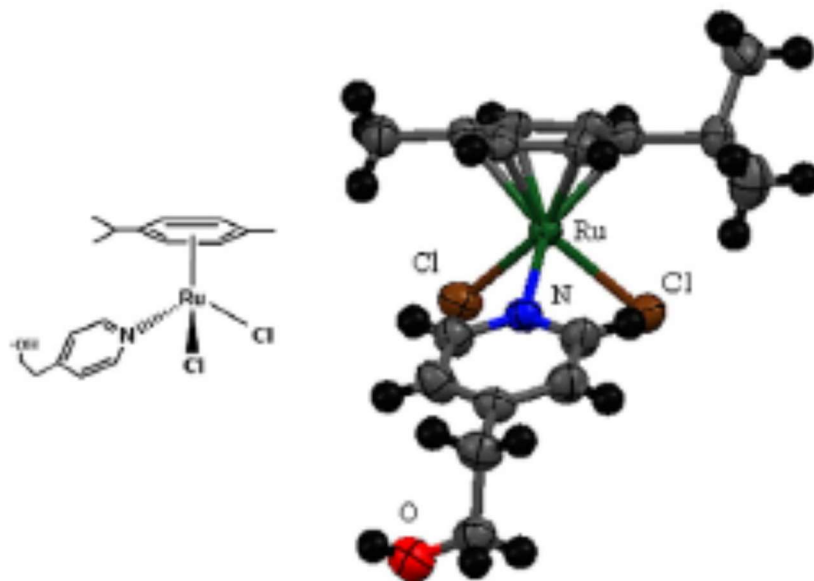
FIGURE 1



717
718
719
720
721
722
723
724
725

726
727
728

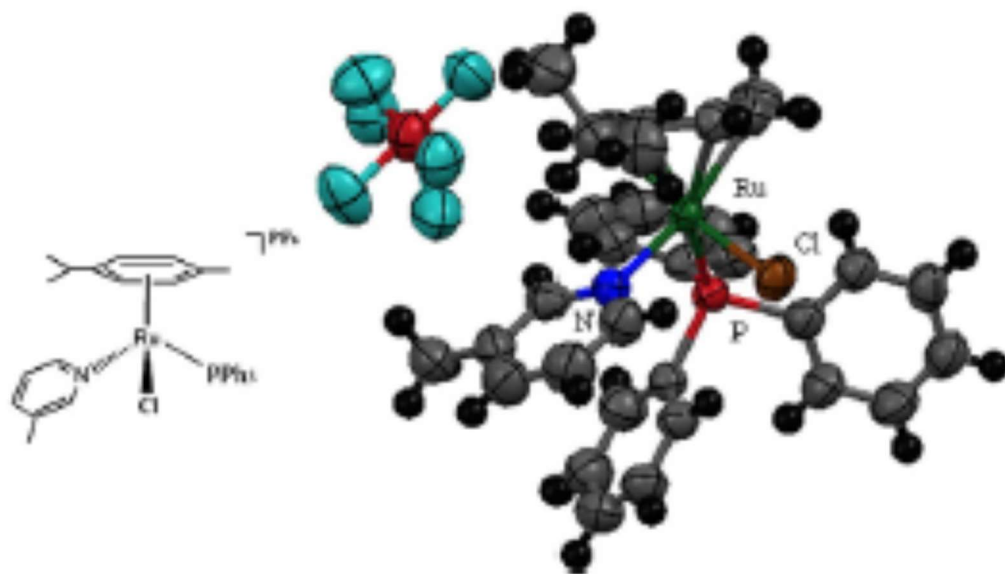
FIGURE 2



729
730
731
732
733
734
735
736
737

FIGURE 3

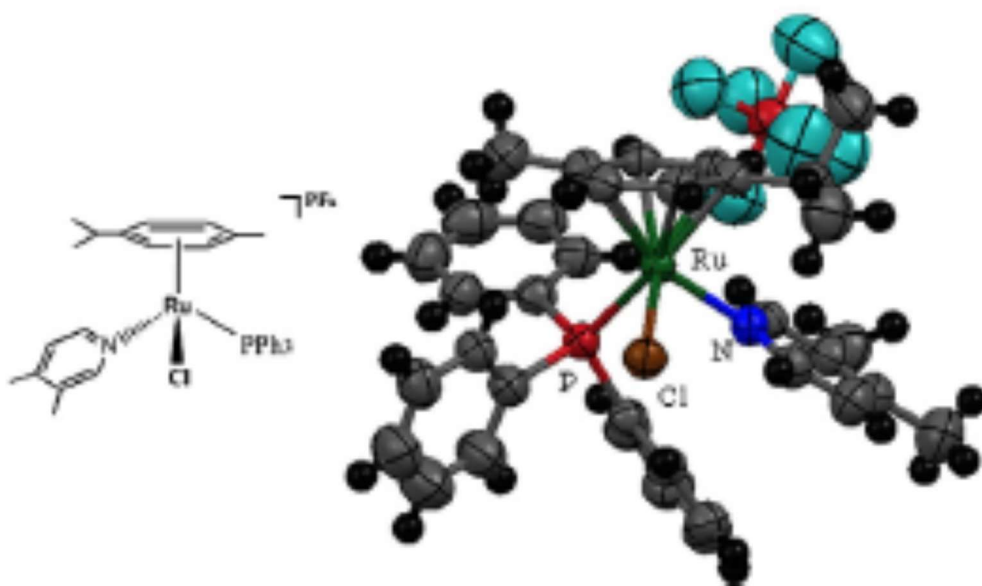
738
739
740



741
742
743
744

745
746
747

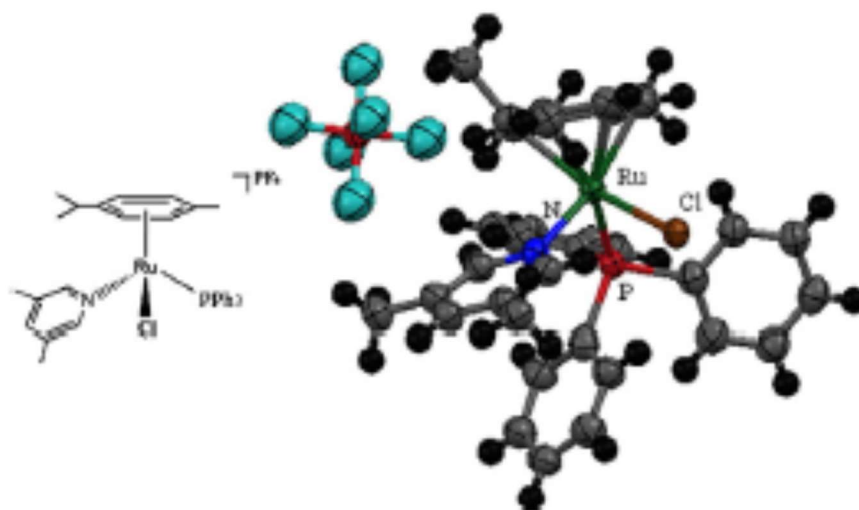
FIGURE 4



748
749
750
751

752
753
754
755

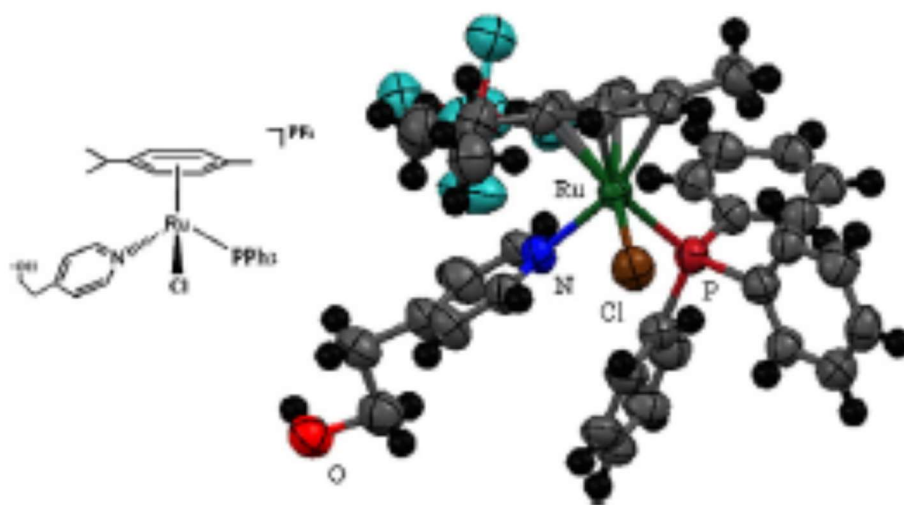
FIGURE 5



756
757

758
759
760

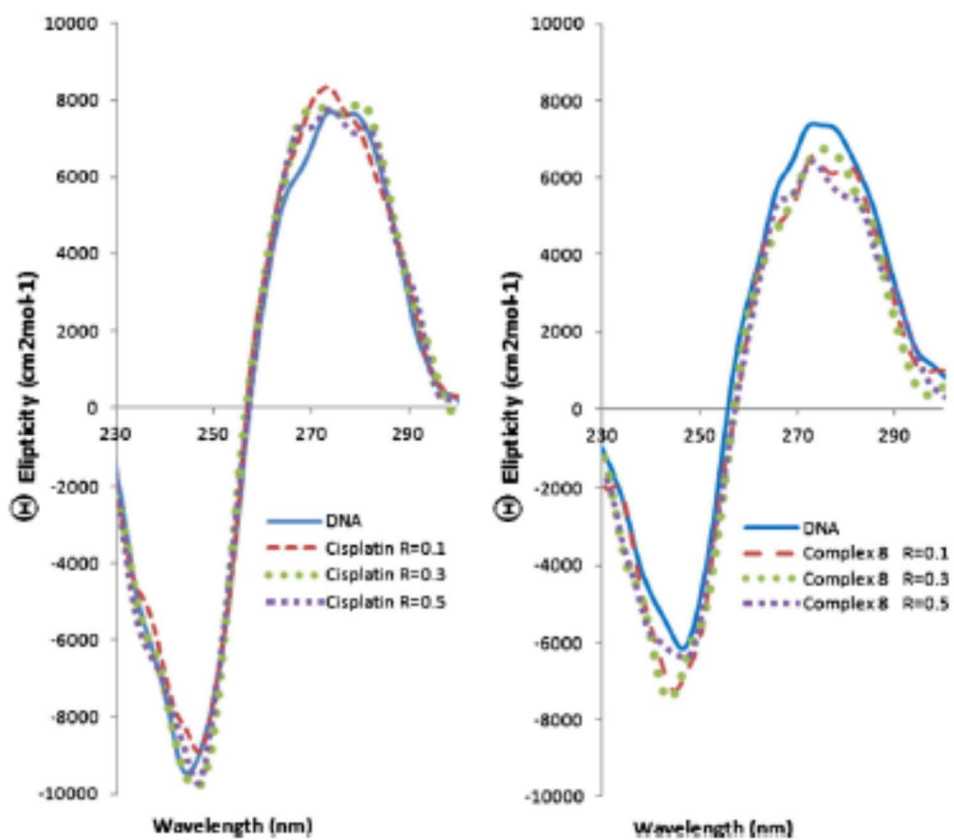
FIGURE 6



761
762

763
764
765

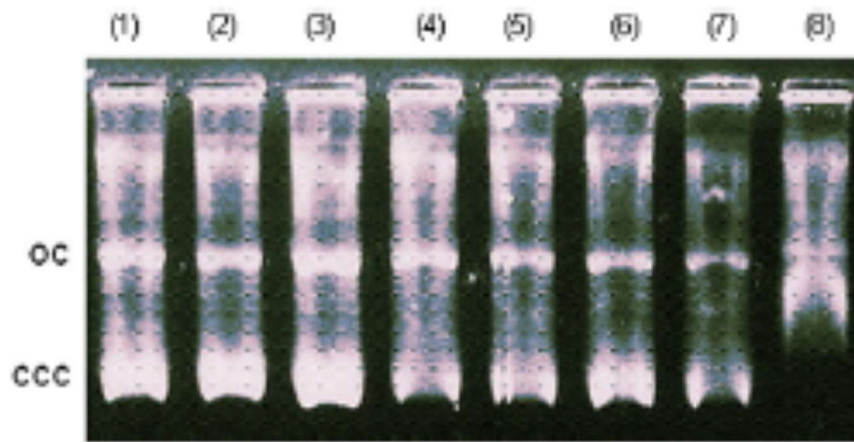
FIGURE 7



766
767

768
769
770

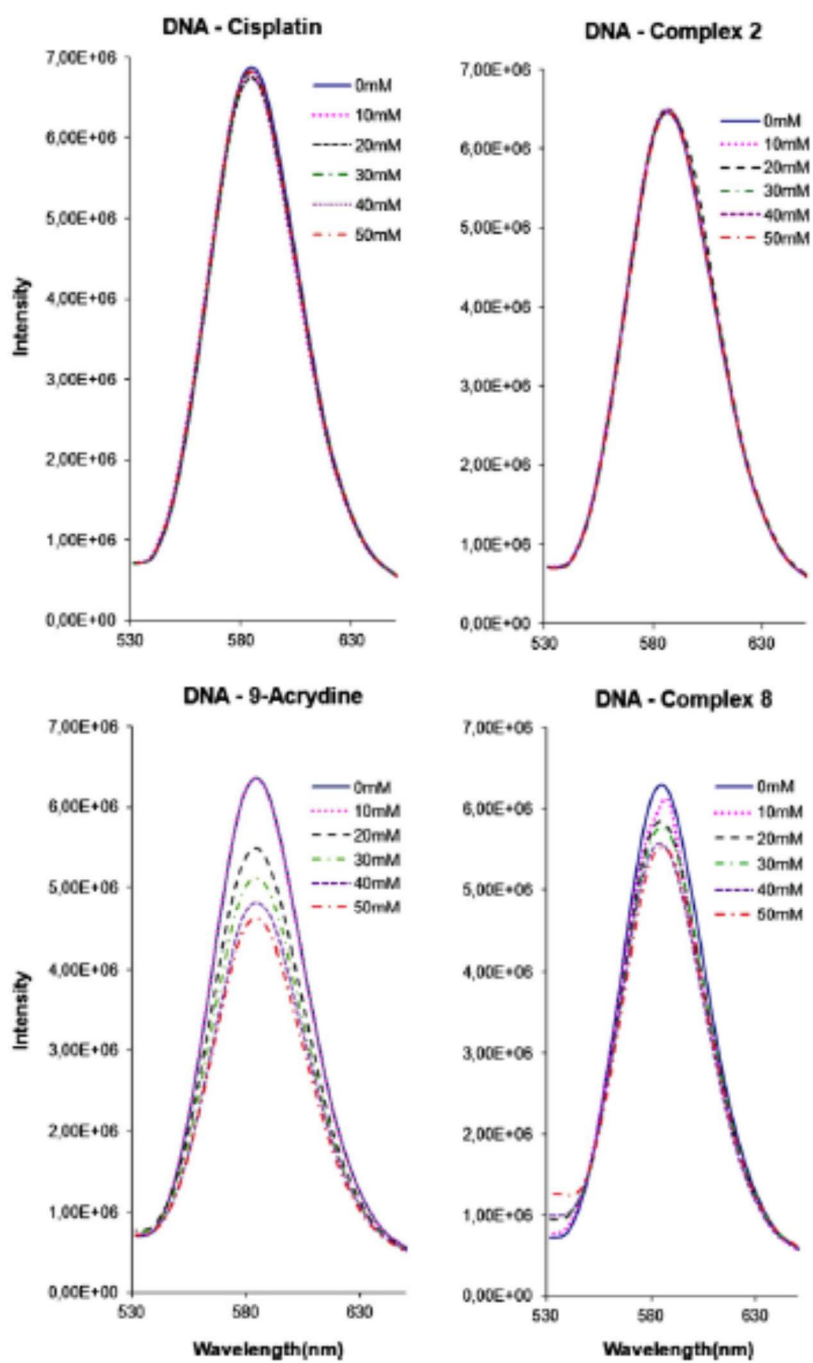
FIGURE 8



771
772
773
774
775
776
777
778

779
780
781

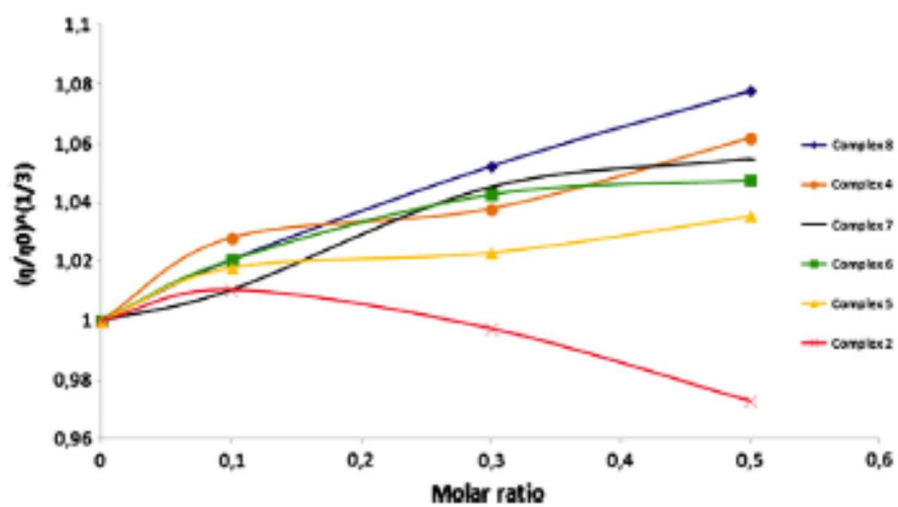
FIGURE 9



782
783
784
785

786
787
788

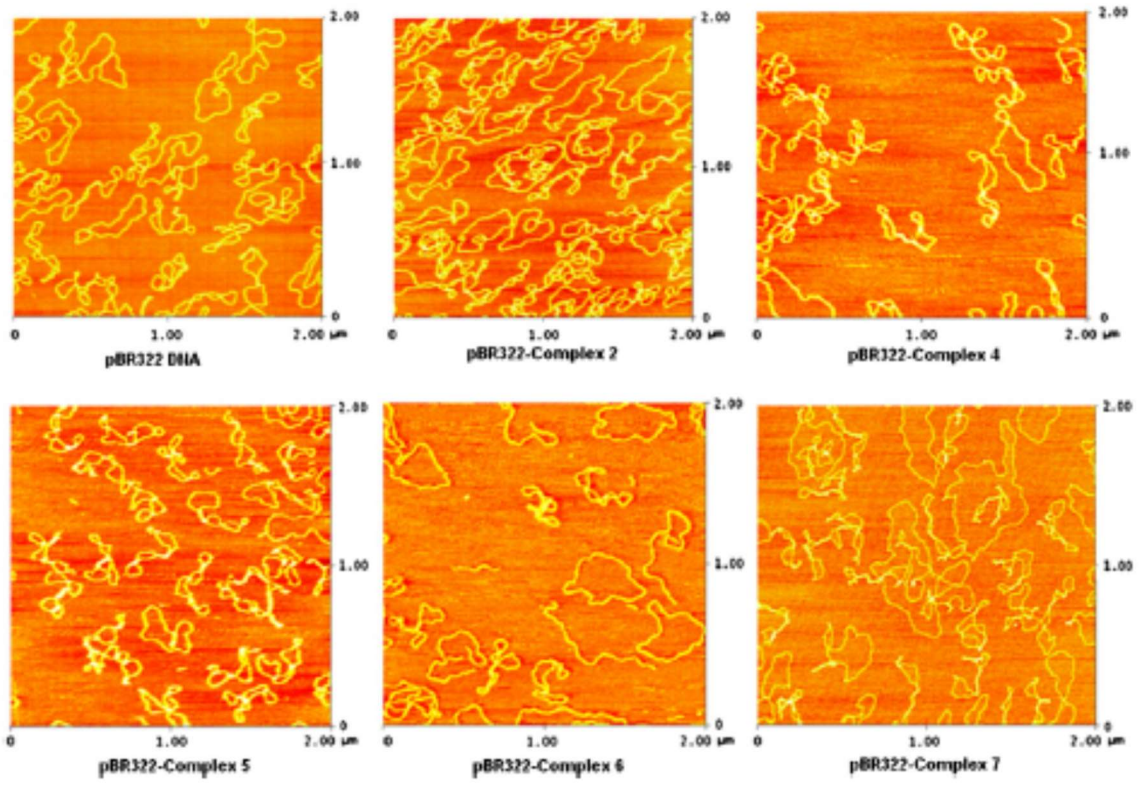
FIGURE 10



789
790
791

792
793
794

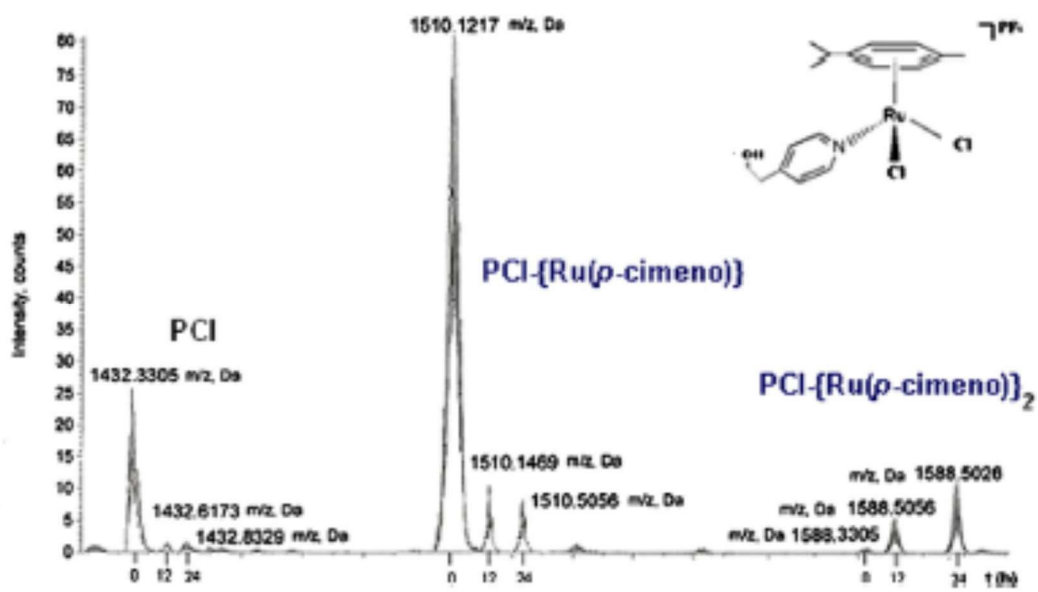
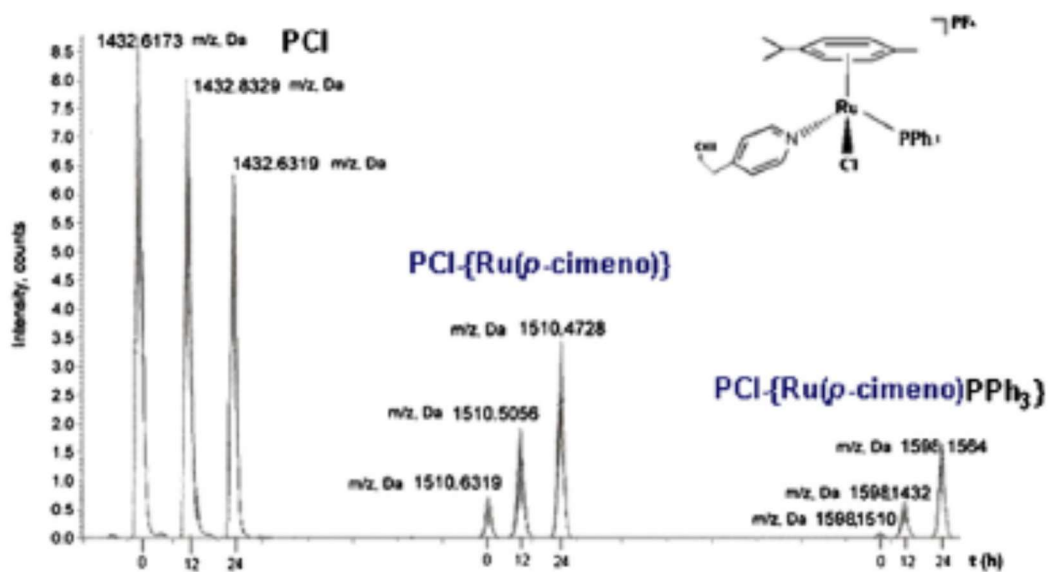
FIGURE 11



795
796
797
798

799
800
801

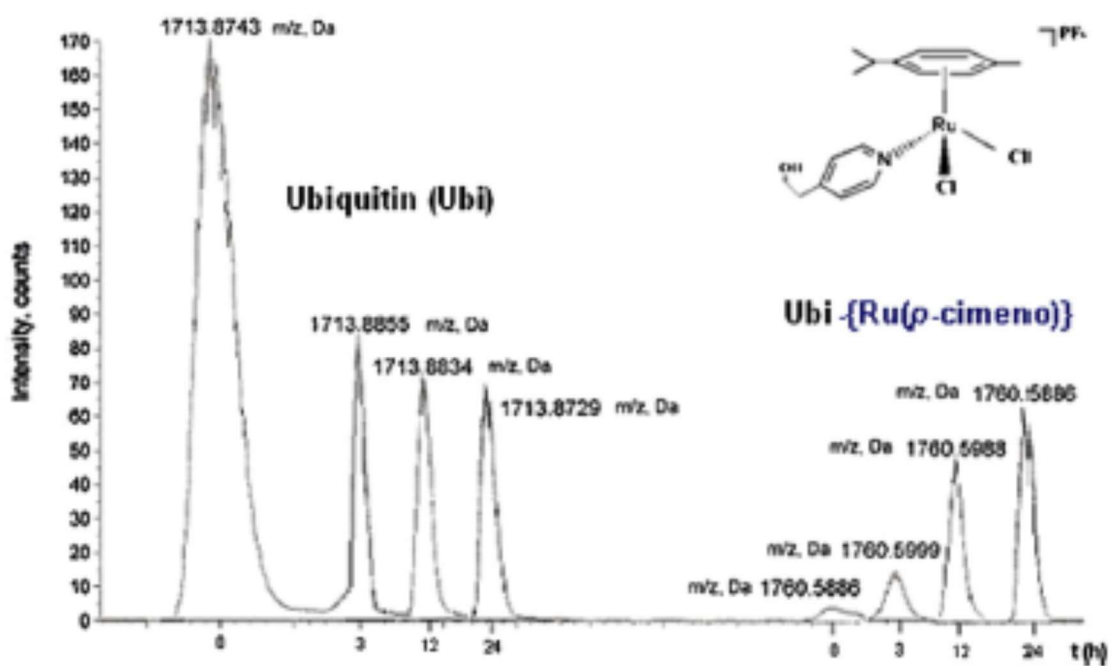
FIGURE 12



802
803

804
805
806

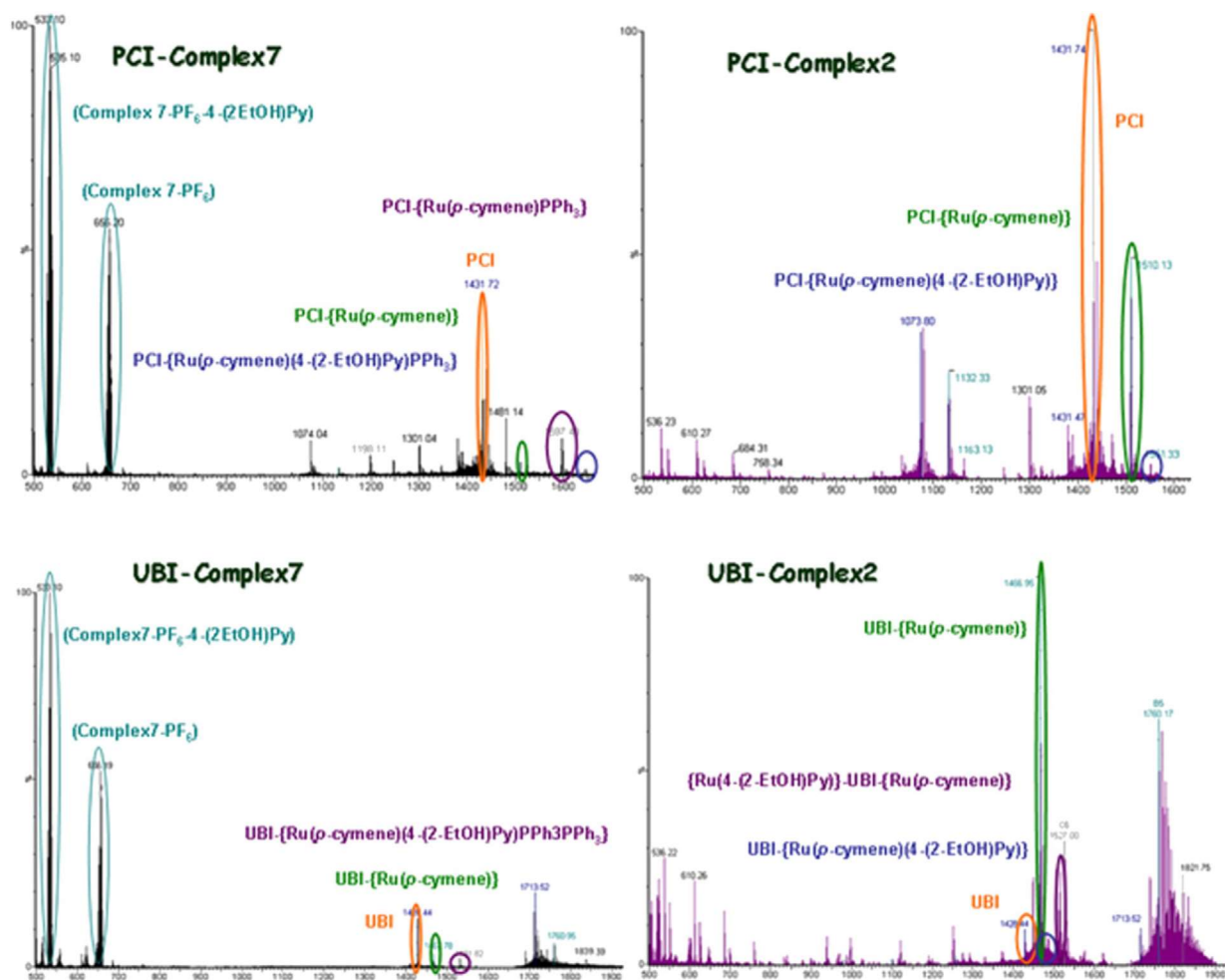
FIGURE 13



807
808

809
810
811

FIGURE 14



812
813
814
815

816 **Table 1.** Summary of crystallographic data.

817

Unit cell dimensions	(2)	(4)	(5)	(6)	(7)
Crystal system	Monoclinic	Orthorhombic	Orthorhombic	Monoclinic	Monoclinic
Space group	$F2_1/c$	$Pbca$	$Pbca$	$F2_1/c$	Cc
a	10.995 (4) Å	18.158 (6) Å	18.494 (2) Å	10.543 (6) Å	10.202 (5) Å
b	8.411 (2) Å	18.521 (6) Å	21.875 (6) Å	18.391 (8) Å	19.636 (5) Å
c	19.960 (7) Å	21.986 (3) Å	21.875 (6) Å	19.901 (8) Å	17.481 (7) Å
α	90°	90°	90°	90°	90°
β	92.31 (2)°	90°	90°	94.62 (2)°	3.00 (2)°
γ	90°	90°	90°	90°	90°

818

819

820

821

822

823 **Table 2.** Cross-section variations of different detected adducts. (a) No DMSO in solution. (b) 2%
824 DMSO in solution.

825
826

Molecule	Adduct	CCS (\AA^2)	Δ CCS %
PCI (a)	–	545	–
PCI (b)	–	569	–
PCI (b)-2	PCI (b)-[Ru(<i>p</i> -cymene)]	584	2.5
PCI (b)-2	PCI (b)-[Ru(<i>p</i> -cymene)PPh ₃]	596	4.5
PCI (a)-7	PCI (a)-[Ru(<i>p</i> -cymene)]	566	3.7
UII (a)	–	1015	–
UII (b)	–	1017	–
UII (b)-2	UII (b)-[Ru(<i>p</i> -cymene)]	1028	1.1
UII (b)-2	UII (b)-[Ru(<i>p</i> -cymene)PPh ₃]	1015	0.02
UII (a)-7	UII (b)-[Ru(<i>p</i> -cymene)]	908	11.7

827
828
829
830
831
832

833 **Table 3.** IC50 values at 24 h for HL60 leukemia tumor cell line.
834
835

Complex	IC ₅₀ (μM)
Complex 2	202
Complex 4	10.1
Complex 5	5.2
Complex 6	5.2
Complex 7	154

836
837
838
839
840